Smart Structures and Systems, *Vol. 33, No. 2 (2024) 165-175*
https://doi.org/10.12989/sss.2024.33.2.165

Two-stage crack identification in an Euler-Bernoulli rotating beam using modal parameters and Genetic Algorithm

Belén Muñoz-Abella*, Lourdes Rubio [a] and Patricia Rubio [b]

Department of Mechanical Engineering, University Carlos III of Madrid, Av. Universidad 30, 28911, Leganés, Madrid, Spain

(*Received September 22, 2023, Revised January 5, 2024, Accepted November 10, 2023*)

Abstract. Rotating beams play a crucial role in representing complex mechanical components that are prevalent in vital sectors like energy and transportation industries. These components are susceptible to the initiation and propagation of cracks, posing a substantial risk to their structural integrity. This study presents a two-stage methodology for detecting the location and estimating the size of an open-edge transverse crack in a rotating Euler-Bernoulli beam with a uniform cross-section. Understanding the dynamic behavior of beams is vital for the effective design and evaluation of their operational performance. In this regard, modal parameters such as natural frequencies and eigenmodes are frequently employed to detect and identify damages in mechanical components. In this instance, the Frobenius method has been employed to determine the first two natural frequencies and corresponding eigenmodes associated with flapwise bending vibration. These calculations have been performed by solving the governing differential equation that describes the motion of the beam. Various parameters have been considered, such as rotational speed, beam slenderness, hub radius, and crack size and location. The effect of the crack has been replaced by a rotational spring whose stiffness represents the increase in local flexibility as a result of the damage presence. In the initial phase of the proposed methodology, a damage index utilizing the slope of the beam's eigenmode has been employed to estimate the location of the crack. After detecting the presence of damage, the size of the crack is determined using a Genetic Algorithm optimization technique. The ultimate goal of the proposed methodology is to enable the development of more suitable and reliable maintenance plans.

Keywords: crack identification; cracked rotating Euler-Bernoulli beam; genetic algorithms; maintenance plans; modal parameters

1. Introduction

Rotating beams play a crucial role in representing complex mechanical components prevalent in vital sectors such as energy, e.g. wind turbine blades or large turbine blades, and transport industries, e.g., helicopter blades. Furthermore, their operational environments, particularly in challenging and aggressive conditions, significantly influence their structural integrity and, subsequently, their optimal performance. Consequently, they are sensitive to cracks that can propagate, resulting in either catastrophic failures or substantial maintenance expenses. It is therefore essential to ensure that sufficient reliability is maintained during operation.

Blades with complex geometries can be effectively modeled using simplified approaches such as the Euler-Bernoulli, Rayleigh, or Timoshenko beam theories. The main differences between these theories revolve around their geometric conditions and the mechanical insights they provide. In cases where the structural slenderness aspect is significant, such as wind turbine blades, the simplified Euler-Bernoulli theory is fully justified (Ahmed and Rifai 2021, Aydin 2013). During blade rotation, a centrifugal force emerges that varies based on the distance from the center of rotation. This force impacts the dynamic behavior in two distinct planes: the plane of rotation (referred to as "chordwise") and the plane outside of it ("flapwise"). It leads to an increase in the natural frequency in both planes. Additionally, the Coriolis acceleration has an effect, exclusively influencing the "chordwise" vibrations (Kim *et al*. 2013).

Understanding the dynamic behavior of beams is essential for their design and operational assessment. Regardless of the characteristics of the beam, the equation used for its dynamic analysis is a fourth-order differential equation with variable coefficients, the solution of which is highly complex. Various authors have addressed the resolution of this problem using diverse approaches. These include the Rayleigh or Rayleigh-Ritz method (Bath 1986), the finite element method (Cheng *et al*. 2011, Liu and Yiang 2014, Valverde-Marcos *et al*. 2022), the Frobenius method (Lee and Lee 2017, Banerjee 2000, Banerjee *et al*. 2006, Muñoz-Abella *et al*. 2022a), the Galerkin method (Chen and Chen 1988) and the differential transform method (Talebi and Ariaei 2015, Özdemir and Kaya 2006). Of particular interest are those approaches that yield closed-form solutions, establishing relationships between variables

*Corresponding author, Ph.D., Associate Professor,
E-mail: mmunoz@ing.uc3m.es
[a] Professor, E-mail: lrubio@ing.uc3m.es
[b] Associate Professor, E-mail: prubio@ing.uc3m.es

ISSN: 1738-1584 (Print), 1738-1991 (Online)

and the dependent parameters. This capability proves invaluable in addressing the inverse problem.

When a crack is present in the beam, it influences both flapwise and chordwise vibrations. However, more comprehensive studies have focused on flapwise vibrations (Masoud and Al-Said 2009). This emphasis is because flapwise vibrations are not coupled with other modes, as is the case with axial and chordwise vibrations (Kim *et al*. 2013).

The reduction in local stiffness caused by the crack's presence impacts transverse displacements, causing them to increase, while also decreasing vibration frequencies. Consequently, two contrasting effects come into play. On one hand, there is heightened flexibility due to the defect, while on the other hand, stiffness increases due to rotational speed. Balancing these opposing effects can potentially complicate damage detection (Valverde-Marcos *et al*. 2022).

Research into cracked rotating beams dates back to the late 1980s. Initial investigations included works by Wauer (1991), who formulated the equation of motion for an Euler-Bernoulli beam by introducing a torsion spring to represent the effect of the crack's flexibility, and Krawczuk (1993), who examined changes in natural frequencies considering a perpetually open crack in an Euler-Bernoulli beam using the finite element method. More recent studies have expanded this field. Liu *et al*. (2015) developed a 3D finite element model to explore diverse aspects of cracked blade behavior, Yashar *et al*. (2018) compared intact and cracked beam behavior using the Rayleigh-Ritz and finite element methods. Meanwhile, Yang *et al*. (2021a, b) conducted a comparative assessment of various crack models employed in such beams. Valverde-Marcos *et al*. (2022) utilized the finite element method to investigate how crack characteristics, including size and location, impact the natural frequencies of the element. Muñoz-Abella *et al*. (2022a) developed two closed-form expressions for low-speed wind turbine rotations. These expressions enable the calculation of the first two natural frequencies of the beam based on all system parameters and the presence of a crack. However, to the authors' knowledge, similar expressions, for other speed ranges, are not available in the literature.

On the other hand, once the above expressions, corresponding to the direct method, are known, the inverse method can be tackled. The most straightforward approach to the inverse problem is to detect the presence or absence of a defect. However, the more intricate aspect, often referred to as identification, goes deeper into the location and/or characteristics of the crack.

Since the 1980s, techniques grounded in modal characteristics such as eigenmodes and natural frequencies have gained extensive use as foundations for detecting and identifying cracks in the domains of civil and mechanical engineering. This is attributed, in part, to their capacity to quantify the severity and position of defects. Regarding the determination of position, the literature features numerous studies employing eigenmodes, along with their slopes and curvatures, to identify defects in the case of non-rotating beams (Nayyar *et al*. 2021, Yazdanpanah *et al*. 2015, Kindova-Petrova 2022). For rotating beams, there is hardly any work to be found. For instance, Banerjee and Pohit (2014) detected of size and location of open-edge transverse crack on a rotating beam using continuous wavelength transform from eigenmodes.

The estimation of crack characteristics based on the knowledge of the natural vibration frequencies of the cracked element constitutes an inverse problem that numerous researchers have engaged. To address this, both response-based and model-based methods find application. Among the former, neural networks (Mohammed *et al*. 2014, Muñoz-Abella *et al*. 2020, Bilotta *et al*. 2023) hold prominence, while within the latter category, conventional optimization techniques (Suh *et al*. 2000, Sekhar 2004, Rubio 2009), those rooted in the formulation of constructive algorithms from the vibration problem's eigenvalues (Fernández-Sáez *et al*. 2017, Rubio *et al*. 2018) and genetic algorithms (Maity and Tripathy 2005, Muñoz-Abella *et al*. 2018, Ramezani and Bahar 2021, Chen *et al*. 2022, Gairola *et al*. 2023) are frequently employed.

In the context of rotating beams, Masoud *et al*. 2009 proposed an identification algorithm grounded in a model of a cracked beam, where they analyzed the variation in lateral frequencies concerning rotational speed to detect crack location. On the other hand, Muñoz-Abella *et al*. (2022b) deployed neural networks to detect and identify cracks in rotating beams, particularly focusing on low rotational speed.

This study presents a two-stage methodology for detecting the location and estimating the size of an open-edge transverse crack in a rotating Euler-Bernoulli beam with a uniform cross-section. In the initial phase of the proposed methodology, a damage index utilizing the slope of the beam's eigenmode has been employed to estimate the location of the crack. After detecting the presence of damage, the size of the crack is determined using a Genetic Algorithm optimization technique.

In conclusion, the proposed methodology allows estimating both the position and depth of the crack based on modal parameters of the cracked beam, which will aid in developing more suitable maintenance plans.

2. Statement of the problem

2.1 Cracked Euler-Bernoulli beam model

This study is focused on analyzing a cracked Euler-Bernoulli rotating beam with the following characteristics. The beam under consideration is a uniform beam of length L with a rectangular cross-section that exhibits double symmetry. The cross-section has a height H and a thickness b. The beam rotates with a constant angular velocity Ω around the Z' axis. The crack, which has a depth a, is located at a distance Xc from the junction point O, where the beam is connected to the hub. Point O serves as the origin of the XYZ reference frame. Fig. 1 illustrates the schematic diagram of the cracked beam, where R represents the radius of the hub attached to the beam. Additionally, it is only considered the transverse deflection along the Z coordinate (flapwise), which is represented by the displace-

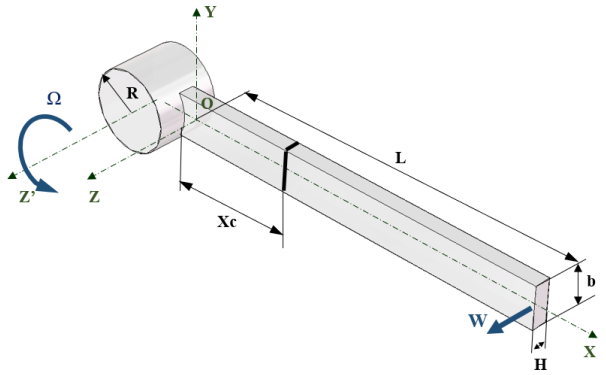

Fig. 1 Scheme of the cracked rotating beam

displacement W (X, t), also shown in Fig. 1.

The governing differential equation for the motion of an intact rotating beam, as expressed in Eq. (1), is a fourth-order equation derived from Newton's Second Law (Lee and Lee 2017, Banerjee *et al*. 2006).

$$\rho A\frac{\partial^2 W(x,t)}{\partial t^2}+\frac{\partial^2}{\partial x^2}\left(EI\frac{\partial^2 W(x,t)}{\partial x^2}\right) -\frac{\partial}{\partial x}\left(P(x)\frac{\partial W(x,t)}{\partial x}\right)=0 \tag{1}$$

being t the time, ρ the density, E the Young's modulus, I the moment of inertia of the section, and A its area. Last, $P(X)$ is the centrifugal force arising in the axial direction due to rotation, and it can be computed using Eq. (2).

$$P(X)=\int_X^L \rho A\Omega^2(X+R)\,dX \tag{2}$$

The conventional method of separating variables can be used to solve Eq. (1), so that

$$W(X,t)=L\overline{W}(X)e^{i\omega t} \tag{3}$$

$\overline{W}(X)$ represents the non-dimensional displacement (see Fig. 1) while ω denotes the vibration natural frequency. Eq. (1) is transformed into Eq. (5) using the dimensionless variables from Eq. (4).

$$\xi=\frac{X}{L};\quad r=\frac{R}{L};\quad \alpha=\frac{a}{H};\quad \mu=\sqrt{\frac{\rho AL^4}{EI}}\,\omega;\quad M=\sqrt{\frac{\rho AL^4}{EI}}\,\Omega \tag{4}$$

$$\frac{d^4\overline{W}(\xi)}{d\xi^4}-M^2\frac{d}{d\xi}\left(\left(r(1-\xi)+\frac{1}{2}(1-\xi^2)\right)\frac{d\overline{W}(\xi)}{d\xi}\right) -\mu^2\omega=0 \tag{5}$$

In the presence of a crack, the governing Eq. (5) is divided into two separate equations, as can be seen in Eq. (6), each corresponding to one side of the crack. These equations are connected by a massless rotational spring, where the stiffness K, according to Chondros *et al*. (1998), represents the inverse of the flexibility introduced by the damage, which is given by Eq. (7).

$$\frac{d^4\overline{W_J}(\xi)}{d\xi^4}-M^2\frac{d}{d\xi}\left(\left(r(1-\xi)+\frac{1}{2}(1-\xi^2)\right)\frac{d\overline{W_J}(\xi)}{d\xi}\right) -\mu^2\omega=0$$
$$\text{J}=1\quad 0\le\xi\le\xi_C$$
$$\text{J}=2\quad \xi_C\le\xi\le 1$$
$$\text{being}\quad \xi_C=\frac{X_C}{L} \tag{6}$$

$$\frac{1}{K}=\frac{6\pi(1-\nu^2)H}{EI}(0.6272\alpha^2-0.04533\alpha^3 +4.5948\alpha^4-9.973\alpha^5+20.2984\alpha^6 -33.031\alpha^7+47.1063\alpha^8 -40.7556\alpha^9+19.6\alpha^{10}) \tag{7}$$

where υ is the material Poisson's ratio.

To solve the aforementioned differential equations, it is necessary to establish four boundary conditions, two for each end of the beam (Eq. (8)) and four compatibility conditions associated with the cracked section (Eq. (9)).

The boundary conditions (Eq. (8)) are those correspond to those of a cantilever beam. The base of the beam (ξ = 0) undergoes neither deflection nor rotation, while at the free end (ξ = 1) it is assumed that there is neither bending moment nor shear force. On the other hand, the compatibility conditions (Eq. (9)) model transverse deflection continuity, slope discontinuity, bending moment continuity and shear force continuity.

$$\overline{W_1}(0)=0\qquad \frac{d\overline{W_1}(0)}{d\xi}=0$$
$$\frac{d^2\overline{W_2}(1)}{d\xi^2}=0\qquad \frac{d^3\overline{W_2}(1)}{d\xi^3}=0 \tag{8}$$

$$\overline{W_1}(\xi_c)=\overline{W_2}(\xi_c)$$
$$\frac{d\overline{W_2}(\xi_c)}{d\xi}-\frac{d\overline{W_1}(\xi_c)}{d\xi}=\frac{EI}{K}\frac{d^2\overline{W_2}(\xi_c)}{d\xi^2}$$
$$\frac{d^2\overline{W_1}(\xi_c)}{d\xi^2}=\frac{d^2\overline{W_2}(\xi_c)}{d\xi^2}$$
$$\frac{d^3\overline{W_1}(\xi_c)}{d\xi^3}=\frac{d^3\overline{W_2}(\xi_c)}{d\xi^3} \tag{9}$$

2.2 Solution of the cracked beam equation of motion

The equation of motion has been solved utilizing the Frobenius series method, which allows the representation of the solution as a power series. This method enables the expression of the solution of the differential equation in the form depicted by Eq. (10).

$$f(\xi,j)=\sum_{n=0}^{\infty}a_{n+1}(j)\cdot\xi^{j+n} \tag{10}$$

The series coefficients are denoted as $a_{n+1}(j)$, while j is an indeterminate exponent. The function $f(\xi,j)$ represents

both $\overline{W_1}$ and $\overline{W_2}$, as they are initially identical before applying the boundary conditions.

By substituting Eq. (10) into Eq. (6), indicial equation and the recurrence relationship can be obtained (Banerjee 2000 and Muñoz-Abella *et al*. 2022a). From them, the solutions of the equations, $F_1(\xi)$ and $F_2(\xi)$, are calculated as a linear combination of $f(\xi,0), f(\xi,1)$, $f(\xi,2)$ and $f(\xi,3)$. Taking into account that $f(\xi,j)$ represents both $\overline{W_1}$ and $\overline{W_2}$, the solutions can be written according Eq. (11).

$$\begin{aligned} F_1(\xi) &= C_1\overline{W_1}(\xi,0) + C_2\overline{W_1}(\xi,1) \\ &\quad + C_3\overline{W_1}(\xi,2) + C_4\overline{W_1}(\xi,2) \\ 0 \le \xi &\le \xi_C \\ F_2(\xi) &= C_5\overline{W_2}(\xi,0) + C_6\overline{W_2}(\xi,1) \\ &\quad + C_7\overline{W_2}(\xi,2) + C_8\overline{W_2}(\xi,2) \\ \xi_C \le \xi &\le 1 \end{aligned} \tag{11}$$

It should be noted that the constants C_1 to C_8 can be computed based on the boundary and compatibility conditions, Eqs. (8) and (9), respectively.

3. Calculation of modal parameters

After presenting the methodology for solving the differential equation in the previous section, the next step involves investigating the changes in modal parameters. Specifically, the behavior of the first two natural frequencies and their corresponding eigenmodes for a given beam and rotational speed are examined. The parameters analyzed are different properties of the beam and the crack, including its location and size.

In this study, a slender beam composed of steel with the following material properties has been considered: modulus of elasticity E = 210 *GPa*, Poisson's ratio v = 0.33, and density ρ = 7850 *kg/m³*.

Moreover, the following parameter values have been considered:

- Slenderness ratio of the beam, S_L = 70, 120, 170, and 220, calculated by Eq. (12).

$$S_L = \sqrt{\frac{AL^2}{I}} \tag{12}$$

- Dimensionless hub radius: r = 0, 0.1, 0.2 and 0.3.
- Dimensionless crack location: ξ_c = 0.1, 0.2, 0.3, 0.4, 0.5, 0.6 0.7, 0.8, and 0.9.
- Dimensionless crack depth: α = 0, 0.1, 0.2, 0.3, 0.4 and 0.5.
- Constant rotation speed: Ω = 0, 50, 100, 150, 200, 250 and 300 rad/s.

Through a convergence analysis, it has been determined that, under the specified operating conditions, the optimal number of terms for the Frobenius series is N = 35. The combination of these parameters has enabled the calculation of 5040 cases, which will be utilized in the development of the crack detection and identification method, the main objective of this study. To gain a deeper understanding of the obtained results for the studied cases, selected examples are presented below, providing a more detailed insight into their behavior.

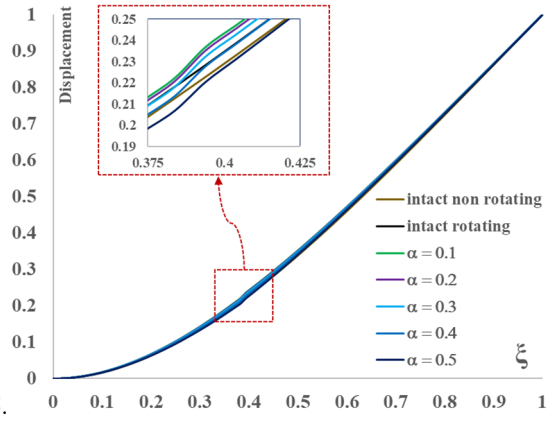

Fig. 2 Eigenmode 1 for ξ_c = 0.4, S_L = 120, r = 0.2, Ω = 200 rad/s, for both the non-rotating and rotating intact beams and for all the crack depths studied

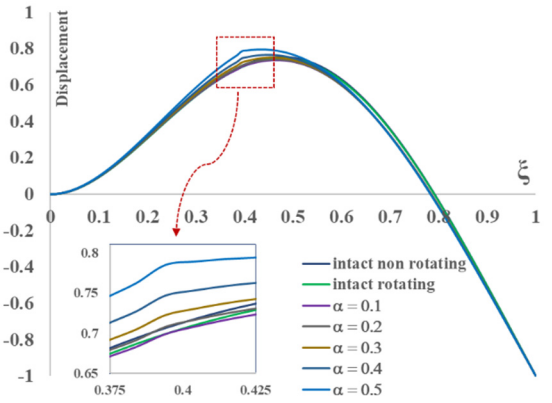

Fig. 3 Eigenmode 2 for ξ_c = 0.4, S_L = 120, r = 0.2, Ω = 200 rad/s, for both the non-rotating and rotating intact beams and all the crack depths studied

3.1 Eigenmodes

Figs. 2 and 3 illustrate the dimensionless eigenmodes corresponding to the first and second natural frequencies, respectively, for the cases with ξ_c = 0.4, S_L = 120, r = 0.2, Ω = 200 rad/s, and the five considered crack depths. The figures also include the eigenmodes of a comparable intact non-rotating beam. It should be noted that for the remaining positions analyzed, the graphical representations exhibit a similar pattern.

For the two eigenmodes shown, a subtle disparity can be observed in the plot of the defective section (ξc = 0.4), depending on the location and depth of the crack. To facilitate a more convenient comparison between the curves, a close-up view of this specific region is also presented in each case. However, despite the differences observed among the above curves as a function of crack depth, these graphs do not provide accurate information for precise estimation of the position and size of the defect.

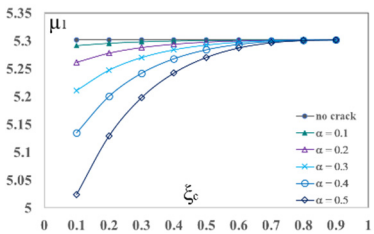

Fig. 4 Variation of μ_1 concerning position and crack size for the specific case of $S_L = 120$, r = 0.2, and $\Omega = 200$ rad/s

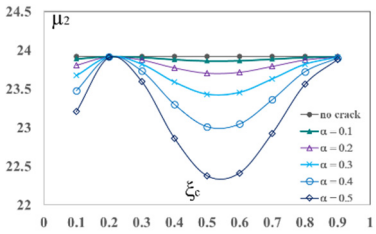

Fig. 5 Variation of μ_2 concerning position and crack size for the specific case of $S_L = 120$, r = 0.2, and $\Omega = 200$ rad/s

3.2 Natural frequencies

In addition, the first two natural frequencies of the 5040 studied cases have been computed. In Figs. 4 and 5, the values of μ_1 and μ_2 (dimensionless natural frequencies) are presented, encompassing all the values of α and ξ_c that were considered, while maintaining average values for the remaining parameters: $S_L = 120$, r = 0.2, and $\Omega = 200$ rad/s. It is worth noting that the general shape of the graphs remains consistent for the remaining values of slenderness, hub radius, and rotation speed.

Regarding the first natural frequency, as depicted in Fig. 4, it is observed that the frequency decreases with an increase in crack size, as expected. Furthermore, the impact of the crack becomes less significant as its distance from the hub increases.

Similarly, for the second natural frequency, as shown in Fig. 5, a decrease in value is observed as the crack size increases. Regarding the influence of the crack location, it is noted that for $\xi c = 0.5$, the minimum frequency value is obtained for all crack sizes. On the contrary, for $\xi c = 0.2$, the frequency remains unaffected by the severity of the defect.

In summary, it can be said that natural frequencies serve as potential parameters for the detection and identification of cracks in rotating beams. However, it is important to note that their effectiveness is highly dependent on their location, as certain positions may not show any perceptible variation in the natural frequencies concerning the size of the defect.

4. Closed-form solutions for the natural frequencies

From the 5040 computed cases, two piecewise closed-form solutions, μ_1 and μ_2, respectively, have been derived to calculate the natural frequencies values. They depend on the following dimensionless parameters: angular velocity, hub radius, beam slenderness, crack location, and depth, according to Eqs. (13) and (14). These expressions will play a crucial role in subsequent sections as they will be used to apply the Genetic Algorithm optimization method for crack identification purposes.

$$\mu_1 = \mu_1(M, r, S_L, \xi_c, \alpha)$$

$$\mu_1 = \begin{cases} \sum_{i=0}^{3}\sum_{j=0}^{1}\sum_{k=0}^{2}\sum_{l=0}^{1}\sum_{m=0}^{2} G_{ijklm}^{11} \cdot M^i \cdot r^j \cdot {S_L}^k \cdot {\xi_c}^l \cdot \alpha^m \;;\; 0.1 \le \xi_c < 0.2 \\ \sum_{i=0}^{3}\sum_{j=0}^{1}\sum_{k=0}^{2}\sum_{l=0}^{1}\sum_{m=0}^{2} G_{ijklm}^{12} \cdot M^i \cdot r^j \cdot {S_L}^k \cdot {\xi_c}^l \cdot \alpha^m \;;\; 0.2 \le \xi_c < 0.3 \\ \sum_{i=0}^{3}\sum_{j=0}^{1}\sum_{k=0}^{2}\sum_{l=0}^{1}\sum_{m=0}^{2} G_{ijklm}^{13} \cdot M^i \cdot r^j \cdot {S_L}^k \cdot {\xi_c}^l \cdot \alpha^m \;;\; 0.3 \le \xi_c < 0.4 \\ \sum_{i=0}^{3}\sum_{j=0}^{1}\sum_{k=0}^{2}\sum_{l=0}^{1}\sum_{m=0}^{2} G_{ijklm}^{14} \cdot M^i \cdot r^j \cdot {S_L}^k \cdot {\xi_c}^l \cdot \alpha^m \;;\; 0.4 \le \xi_c < 0.5 \\ \sum_{i=0}^{3}\sum_{j=0}^{1}\sum_{k=0}^{2}\sum_{l=0}^{1}\sum_{m=0}^{2} G_{ijklm}^{15} \cdot M^i \cdot r^j \cdot {S_L}^k \cdot {\xi_c}^l \cdot \alpha^m \;;\; 0.5 \le \xi_c < 0.6 \\ \sum_{i=0}^{3}\sum_{j=0}^{1}\sum_{k=0}^{2}\sum_{l=0}^{1}\sum_{m=0}^{2} G_{ijklm}^{16} \cdot M^i \cdot r^j \cdot {S_L}^k \cdot {\xi_c}^l \cdot \alpha^m \;;\; 0.6 \le \xi_c < 0.7 \\ \sum_{i=0}^{3}\sum_{j=0}^{1}\sum_{k=0}^{2}\sum_{l=0}^{1}\sum_{m=0}^{2} G_{ijklm}^{17} \cdot M^i \cdot r^j \cdot {S_L}^k \cdot {\xi_c}^l \cdot \alpha^m \;;\; 0.7 \le \xi_c < 0.8 \\ \sum_{i=0}^{3}\sum_{j=0}^{1}\sum_{k=0}^{2}\sum_{l=0}^{1}\sum_{m=0}^{2} G_{ijklm}^{18} \cdot M^i \cdot r^j \cdot {S_L}^k \cdot {\xi_c}^l \cdot \alpha^m \;;\; 0.8 \le \xi_c \le 0.9 \end{cases} \tag{13}$$

$$\mu_2 = \mu_2(M, r, S_L, \xi_c, \alpha)$$

$$\mu_2 = \begin{cases} \sum_{i=0}^{3}\sum_{j=0}^{1}\sum_{k=0}^{2}\sum_{l=0}^{1}\sum_{m=0}^{2} G_{ijklm}^{21} \cdot M^i \cdot r^j \cdot {S_L}^k \cdot {\xi_c}^l \cdot \alpha^m \;;\; 0.1 \le \xi_c < 0.2 \\ \sum_{i=0}^{3}\sum_{j=0}^{1}\sum_{k=0}^{2}\sum_{l=0}^{1}\sum_{m=0}^{2} G_{ijklm}^{22} \cdot M^i \cdot r^j \cdot {S_L}^k \cdot {\xi_c}^l \cdot \alpha^m \;;\; 0.2 \le \xi_c < 0.3 \\ \sum_{i=0}^{3}\sum_{j=0}^{1}\sum_{k=0}^{2}\sum_{l=0}^{1}\sum_{m=0}^{2} G_{ijklm}^{23} \cdot M^i \cdot r^j \cdot {S_L}^k \cdot {\xi_c}^l \cdot \alpha^m \;;\; 0.3 \le \xi_c < 0.4 \\ \sum_{i=0}^{3}\sum_{j=0}^{1}\sum_{k=0}^{2}\sum_{l=0}^{1}\sum_{m=0}^{2} G_{ijklm}^{24} \cdot M^i \cdot r^j \cdot {S_L}^k \cdot {\xi_c}^l \cdot \alpha^m \;;\; 0.4 \le \xi_c < 0.5 \\ \sum_{i=0}^{3}\sum_{j=0}^{1}\sum_{k=0}^{2}\sum_{l=0}^{1}\sum_{m=0}^{2} G_{ijklm}^{25} \cdot M^i \cdot r^j \cdot {S_L}^k \cdot {\xi_c}^l \cdot \alpha^m \;;\; 0.5 \le \xi_c < 0.6 \\ \sum_{i=0}^{3}\sum_{j=0}^{1}\sum_{k=0}^{2}\sum_{l=0}^{1}\sum_{m=0}^{2} G_{ijklm}^{26} \cdot M^i \cdot r^j \cdot {S_L}^k \cdot {\xi_c}^l \cdot \alpha^m \;;\; 0.6 \le \xi_c < 0.7 \\ \sum_{i=0}^{3}\sum_{j=0}^{1}\sum_{k=0}^{2}\sum_{l=0}^{1}\sum_{m=0}^{2} G_{ijklm}^{27} \cdot M^i \cdot r^j \cdot {S_L}^k \cdot {\xi_c}^l \cdot \alpha^m \;;\; 0.7 \le \xi_c < 0.8 \\ \sum_{i=0}^{3}\sum_{j=0}^{1}\sum_{k=0}^{2}\sum_{l=0}^{1}\sum_{m=0}^{2} G_{ijklm}^{28} \cdot M^i \cdot r^j \cdot {S_L}^k \cdot {\xi_c}^l \cdot \alpha^m \;;\; 0.8 \le \xi_c \le 0.9 \end{cases} \tag{14}$$

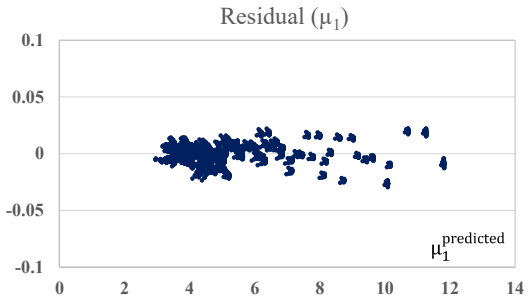

Fig. 6 Residual plot for the μ1 fitting

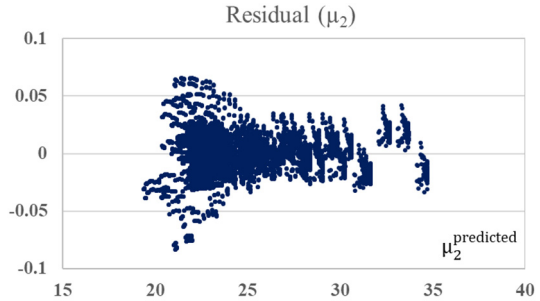

Fig. 7 Residual plot for the μ2 fitting

As can be seen in Eqs. (13) and (14), the functions μ_1 and μ_2 have been fitted piecewise using polynomial expressions through multiple regression techniques. The degrees of the polynomials are represented by i, j, k, l and m, corresponding to M, r, S_L, ξ_c, and α, respectively. Additionally, the coefficients of the fits, denoted as G_{ijklm}^{1*} and G_{ijklm}^{2*}, with * ranging from 1 to 8, can be found in a public repository (Muñoz-Abella *et al*. 2023).

Figs. 6 and 7 depict the residual plots for the variables μ_1 and μ_2, respectively, which were computed using Eq. (15).

$$residual(\mu_{**}) = \mu_{**}^{actual} - \mu_{**}^{predicted} \quad here \;\; ** = 1,2 \tag{15}$$

As can be seen, for μ_1, the absolute value of the residuals is below 0.03, while for μ_2, it is below 0.08. Furthermore, to assess the quality of the fit, the mean square error (MSE), according to Eq. (16), and the coefficient R^2 have been employed. In Table 1, the calculated parameters are shown.

Table 1 MSE and R2 of the natural frequencies fitting

	μ_1	μ_2
MSE	$2.12 \cdot 10^{-6}$	$4.92 \cdot 10^{-7}$
R^2	0.999	0.999

Based on the obtained values, it can be concluded that the derived closed-form expressions are valid for estimating the first two natural frequencies as a function of the angular velocity, hub radius, beam slenderness, crack location, and depth.

$$MSE = \frac{1}{5040}\sum_{i=1}^{5040}\left(\mu_{**}^{actual} - \mu_{**}^{predicted}\right)^2 \tag{16}$$

5. Two-stage crack identification

In the previous sections, the direct problem has been addressed, which involves calculating the values of the natural frequencies based on the system and crack

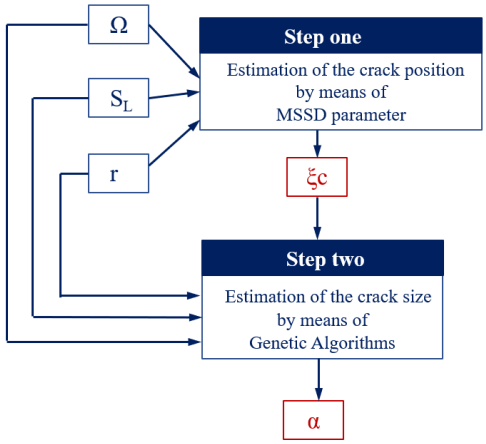

Fig. 8 Flow chart of the proposed two-stage identification methodology

parameters. The next step, explained in the current section, is to approach the inverse problem, which consists of a two-stage identification method. First, the location of the crack is estimated, and then its size is determined. Fig. 8 shows a flow chart of the proposed two-stage identification methodology.

5.1 Step one. Estimation of the crack position

In the literature, various methods based on the analysis of eigenmodes and their derivatives can be found for locating defects in structures and mechanical components. In this study, the "Mode shape slope difference" (MSSD), method proposed by Kindova-Petrova (2022) for non-rotating beams has been chosen due to its simplicity and the fact that it does not require the eigenmodes of an intact beam as a reference. The MSSD is calculated using Eq. (17) to Eq. (20). The positions of cracks are located identifying the points with the maximum values of MSSD.

$$MSSD(k) = \frac{|\Delta(\Phi_k)'|}{max|\Delta(\Phi_{k=1,\ ,n})'|} \tag{17}$$

$$\Delta(\Phi_k)' = \left(\Phi_{k,p1}\right)' - \left(\Phi_{k,p2}\right)' \tag{18}$$

$$\left(\Phi_{k,p1}\right)' = \frac{-3\Phi_k + 4\Phi_{k+1} - \Phi_{k+2}}{2h_m} \tag{19}$$

$$\left(\Phi_{k,p2}\right)' = \frac{\Phi_{k-2} - 4\Phi_{k-1} + 3\Phi_k}{2h_m} \tag{20}$$

In the proposed method, the MSSD parameter is calculated by comparing the slopes of the eigenmodes at different points. The eigenmode is represented by the symbol Φ, and k denotes each of the points ξ used to calculate the eigenmode. The parameter h_m represents the distance between two consecutive k points. To facilitate comprehension, Fig. 9 shows the schematic of a first eigenmode, in which these parameters are noted. The scheme is also applicable to the second eigenmode.

The MSSD parameter quantifies the difference between

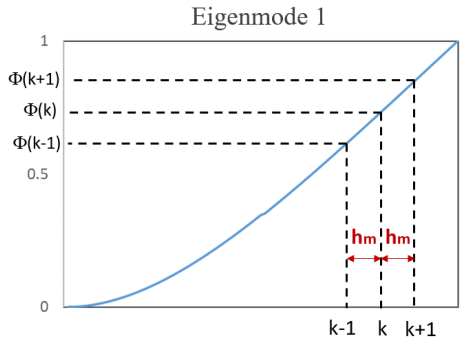

Fig. 9 Schematic of a first eigenmode

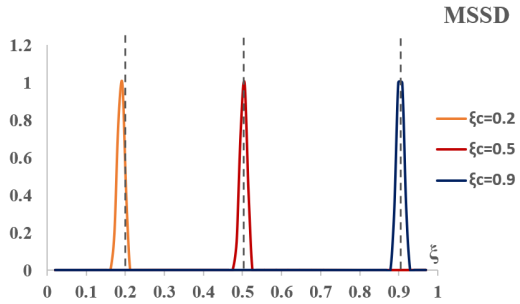

Fig. 10 MSSD for SL = 120, r = 0.2, and Ω = 200 rad/s, with crack positions ξc = 0.2, 0.5 and 0.9

the slopes of the eigenmodes calculated using two numerical approximation formulas. Specifically, Eq. (19) employs the prior approximation "p1", while Eq. (20) utilizes the posterior approximation "p2". By evaluating the MSSD, one can identify the position of a potential crack by locating the points with maximum deviations in the slopes of the eigenmodes.

As an illustrative example, Fig. 10 displays the MSSD parameter calculated from the first eigenmode, using 100 points. This is shown for the cases where S_L = 120, r = 0.2, and Ω = 200 rad/s, with crack positions ξ_c = 0.2, 0.5, and 0.9. These positions were chosen as they represent the most challenging cases to detect based on the values of the natural frequencies (see Figs. 4-5).

It is important to note that since the MSSD parameter is dimensionless, the obtained graphs for the same crack position are identical regardless of the beam's slenderness, crack size, hub radius, and angular velocity. Additionally, the MSSD graphs remain the same regardless of the specific eigenmode used to calculate them.

Upon using 100 points to calculate the eigenmodes, it is observed that at ξ_c = 0.2, the estimated position is $\xi_{c,est}$ = 0.19. For ξ_c = 0.5, the estimated location corresponds to $\xi_{c,est}$ = 0.5, and at ξ_c = 0.9, the estimated position is $\xi_{c,est}$ = 0.9. In conclusion, using 100 points, the maximum error is found to be less than 5%.

Therefore, the MSSD parameter can be considered a reliable indicator to determine the presence and position of a crack, if any, where the accuracy of crack location depends primarily on the number of data points used to characterize the beam's eigenmode.

Table 2 GA parameters

Parameter	Value
Population size	50
Crossover function	Scattered
Crossover fraction	0.8
Elite count	3
Scaling function	Rank
Selection function	Stochastic uniform
Mutation function	Adaptive feasible
Mutation probability	0.01

5.2 Step two. Estimation of the crack size

After estimating the position of the crack, the subsequent step is to determine its depth. In the proposed methodology, the crack identification problem is addressed using the Genetic Algorithm optimization technique (GA).

As widely known, GAs are general-purpose optimization algorithms inspired by Darwin's theory of evolution and natural selection. They explore a solution space to find the optimal solution for a given problem.

In a GA, potential solutions are encoded as chromosomes. The algorithm begins by creating an initial population of potential solutions and iteratively evolves them over multiple generations to find improved solutions. Each individual in the population is evaluated based on a fitness value, which is derived from the objective function of the problem. In each generation, new individuals are created through a selection process that favors the better-adapted individuals from the previous generation. This process emulates the principle of "survival of the fittest" observed in the natural world.

The proposed GA is developed under the MATLAB environment (Matlab 2023), with which the fitness function, *f*, as can be seen in Eq. (21), should be minimized.

Where μ_1^c and μ_2^c are the first and second, respectively, dimensionless natural frequencies, calculated using Eqs. (13) and (14), and μ_1^m and μ_2^m are the measured values in a real system of the same variables. The parameters of the developed GA are shown in Table 2.

6. Numerical experiments

6.1 Comparison with data used to calculate the closed-form expressions

To illustrate the two-stage crack identification procedure, several numerical experiments have been conducted. In the initial set of experiments, ten cases have randomly been selected from the data set of 5040 computed cases used to calculate the closed-form expressions. The properties of the chosen cases and the obtained results can be found in Table 3. In all cases, to ensure consistent results, each case has been executed five times over 50 generations. It can be observed the estimated values for the position ($\xi c^{estimated}$) and depth ($\alpha^{estimated}$), calculated as the average of the results from the five runs. Additionally, it can be found the differences between actual and estimated values for both variables.

As can be seen in Table 3, the differences in crack dimensionless location estimation are consistently below 0.01. Naturally, the precision of crack location detection is mainly contingent on the number of data points (k) used to characterize the beam's eigenmode. A greater number of data points leads to a narrower margin between the actual and estimated values. Regarding the dimensionless size estimation, the differences remain below 0.02.

6.2 Comparison with data different from those used to calculate the closed-form expressions

Secondly, the same procedure in the previous paragraph has been applied to ten random different cases from those

$$\begin{aligned} &if\ \xi_c \le 0.3\ f = 0.75 * (\mu_1^c - \mu_1^a)^2 + 0.25 * (\mu_2^c - \mu_2^a)^2 \\ &if\ \ 0.3 \le \xi_c < 0.8\ f = 0.25 * (\mu_1^c - \mu_1^a)^2 + 0.75 * (\mu_2^c - \mu_2^a)^2 \\ &if\ \ 0.8 \le \xi_c\ f = 0.15 * (\mu_1^c - \mu_1^a)^2 + 0.85 * (\mu_2^c - \mu_2^a)^2 \end{aligned} \tag{21}$$

Table 3 Numerical experiment for 10 random cases from data used for developing the closed-form expressions

Case	Ω (rad/s)	S_L	r	ξc^{actual}	$\xi c^{estimated}$	$\xi c^{actual} - \xi c^{estimated}$	α^{actual}	$\alpha^{estimated}$	$\alpha^{actual} - \alpha^{estimated}$
1a	150	120	0.2	0.7	0.707	**-0.007**	0.4	0.393	**0.007**
2a	150	120	0	0.5	0.505	**-0.005**	0.5	0.498	**0.002**
3a	50	70	0	0.2	0.192	**0.008**	0.4	0.382	**0.018**
4a	200	70	0	0.2	0.192	**0.008**	0.2	0.194	**0.006**
5a	50	120	0.3	0.7	0.697	**0.003**	0.3	0.291	**0.009**
6a	300	220	0.2	0.8	0.798	**0.002**	0.4	0.381	**0.019**
7a	100	220	0.3	0.8	0.798	**0.002**	0.3	0.297	**0.003**
8a	50	70	0.1	0.9	0.899	**0.001**	0.5	0.488	**0.012**
9a	250	70	0.1	0.9	0.899	**0.001**	0.3	0.288	**0.012**
10a	300	70	0	0.3	0.303	**-0.003**	0.1	0.111	**-0.011**

Table 4 Numerical experiment for 10 random cases from data different from those used for developing the closed-form expressions

Case	Ω (rad/s)	S_L	r	ξ_c^{actual}	$\xi_c^{estimated}$	$\xi_c^{actual} - \xi_c^{estimated}$	α^{actual}	$\alpha^{estimated}$	$\alpha^{actual} - \alpha^{estimated}$
1b	297	156	0.045	0.65	0.646	**0.004**	0.35	0.344	**0.006**
2b	154	92	0.26	0.74	0.737	**0.003**	0.17	0.178	**-0.008**
3b	101	200	0.29	0.33	0.313	**0.017**	0.42	0.445	**-0.025**
4b	142	135	0.14	0.27	0.263	**0.007**	0.31	0.313	**-0.003**
5b	62	82	0.06	0.48	0.475	**0.005**	0.44	0.437	**0.003**
6b	212	95	0.18	0.55	0.545	**0.005**	0.27	0.267	**0.003**
7b	85	166	0.28	0.17	0.171	**-0.001**	0.12	0.123	**-0.003**
8b	292	128	0.18	0.38	0.384	**-0.004**	0.25	0.246	**0.004**
9b	182	95	0.23	0.77	0.767	**0.003**	0.32	0.298	**0.022**
10b	115	210	0.12	0.58	0.585	**-0.005**	0.04	0.050	**-0.01**

Table 5 α differences obtained from the sensitivity analysis

Case	Ω (rad/s)	S_L	r	ξ_c^{actual}	α^{actual}	$\alpha^{estimated}$	$\alpha^{actual} - \alpha^{estimated}$
1b	297	156	0.045	0.65	0.35	0.38	**-0.03**
2b	154	92	0.26	0.74	0.17	0.11	**0.06**
3b	101	200	0.29	0.33	0.42	0.49	**-0.07**
4b	142	135	0.14	0.27	0.31	0.24	**0.07**
5b	62	82	0.06	0.48	0.44	0.39	**0.05**

used to determine the closed-form expressions. Those cases and their results can be seen in Table 4.

According to the values shown in Table 4, both, for the estimation of the position and the depth of the crack, the differences found in Table 4 are slightly larger than those calculated for the data shown in Table 3, but in neither of the two variables they exceed 0.025.

6.3 Robustness of the proposed methodology

The ultimate goal of this methodology is its application to real-world systems. To simulate real measurements of a rotating beam, sensitivity to errors has been examined. To achieve this, Gaussian random noise has been generated and incorporated into the responses of the beam model, specifically affecting the μ_1 and μ_2 inputs. Noise levels of 5% relative to their respective values have been introduced for analysis.

On the other hand, it is necessary to emphasize that the crack position is obtained in the first stage of the methodology and serves as an input for the second phase (GA), and its accuracy mainly depends on the number of points used to calculate the eigenmodes. For that reason, a 5% Gaussian noise has also been introduced to this variable to subsequently estimate the crack depth, α.

The sensitivity analysis has been calculated for five cases from the previous section. Table 5 shows the obtained differences between actual and estimated values in this analysis for the crack size.

As shown in Table 5, the differences between the actual and estimated dimensionless crack depths do not exceed 0.07 in the examined cases. Although it's true that in the most challenging scenarios, the differences are notably higher compared to previous estimations without additional error, it can still be considered satisfactory for real-world applications, allowing for the establishment of more reliable maintenance plans, which constitutes the ultimate goal of this study.

7. Conclusions

This work presents a two-stage methodology that allows estimating the position and size of a crack in a uniformly sectioned rotating Euler-Bernoulli beam turning with a constant angular speed. In the first step, based on the formulation and solution, using the Frobenius method, of the equation governing the motion of the beam, two piecewise closed-form expressions have been developed. These expressions enable the calculation of the first two natural frequencies of the system as functions of angular velocity, hub radius, beam slenderness, and position and depth of the defect. It has been found that the fitting results of these expressions closely align with the original results obtained through the solution of the motion equation. These expressions offer the advantage of computing the modal parameters of the beam, based on its characteristics and the crack properties, without the need to solve the governing differential equation, employing a faster and simpler procedure. Additionally, they serve as the foundation for the presented two-stage methodology.

Based on the developed closed-form expressions, the methodology first allows estimating the crack position through the MSSD parameter. This parameter depends on

the slope of any of the beam's eigenmodes, and it is independent of angular velocity and crack depth. Subsequently, by applying the methodology, the crack size can be calculated using GA techniques. The following conclusions can be drawn from the obtained results:

- The accuracy of the crack position estimation depends primarily on the points chosen to calculate the beam's eigenmodes.
- The GA results are very good for the values used in the development of the closed-form expressions and slightly less accurate, but still acceptable, for values not used in their development.
- To simulate a real system, the methodology has been tested with input values to which a 5% Gaussian error has been applied. It has been found that although the differences are higher than in theoretical previous cases, they are sufficiently small to consider the methodology applicable to real systems to achieve appropriate maintenance plans.

In summary, this work presents a two-stage methodology for identifying cracks in Euler-Bernoulli rotating beams. It enables the estimation of both the position and depth of the crack by utilizing modal parameters of the cracked beam in conjunction with genetic algorithm techniques. Implementing this approach in real-world systems will be instrumental in devising more effective maintenance plans.

Acknowledgments

This work was supported by the "Agencia Estatal de Investigacion" (AEI) of the Government of Spain through the project:
PID2019-104799GB-I00/AEI/10.13039/501100011033.

References

Ahmed, A.M. and Rifai, A.M. (2021), "Euler-Bernoulli and Timoshenko beam theories. Analytical and numerical comprehensive revision", *Eur. J. Eng. Sci. Tech.*, **6**(7), 20-32. https://doi.org/10.24018/ejeng.2021.6.7.2626

Aydin, K. (2013), "Influence of crack and slenderness ratio on the eigenfrequencies of Euler-Bernoulli and Timoshenko beams", *Mech. Adv. Mater. Struct.*, **20**, 339-352. https://doi.org/10.1080/15376494.2011.627635

Banerjee, J.R. (2000), "Free vibration of centrifugally stiffened uniform and tapered beams using the Dynamic stiffness method", *J. Sound Vib.*, 233(5), 857-875. https://doi.org/10.1006/jsvi.1999.2855

Banerjee, A. and Pohit, G. (2014), "Crack detection in rotating cantilever beam by Continuous Wavelet Transform", *Appl. Mech. Mater.*, **592-594**, 2021-2025. https://doi.org/10.4028/www.scientific.net/AMM.592-594.2021

Banerjee, J.R., Su, H. and Jackson, D.R. (2006), "Free vibration of rotating tapered beams using the dynamic stiffness method", *J. Sound Vib.*, **4-5**, 1034-1054. https://doi.org/10.1016/j.jsv.2006.06.040

Bath, R.B. (1986), "Transverse vibrations of a rotating uniform cantilever beam with tip mass as predicted by using beam characteristic orthogonal polynomials in the Rayleigh-Ritz method", *J. Sound Vib.*, **105**(2), 199-210. https://doi.org/10.1016/0022-460X(86)90149-5

Bilotta, A, Morassi, A. and Turco, E. (2023), "Damage identification for steel-concrete composite beams through convolutional neural networks", *J. Vib. Control*, **30**(3-4), 876-889. https://doi.org/10.1177/10775463231152926

Chen, L.W. and Chen, C.L. (1988), "Vibration and stability of cracked thick rotating blades", *Comput. Struct.*, **28**(1), 67-74. https://doi.org/10.1016/0045-7949(88)90093-4

Chen, H., Yong, H. and Zhou, Y. (2022), "Crack detection in bulk superconductor using genetic algorithm", *Eng. Fract. Mech.*, **265**, 108372. https://doi.org/10.1016/j.engfracmech.2022.108372

Cheng, Y., Yu, Z., Wu, X. and Yuan, Y. (2011), "Vibration analysis of a cracked rotating tapered beam using the p-version finite element method", *Finite Elem. Anal. Des.*, **47**, 825-834. https://doi.org/10.1016/j.finel.2011.02.013

Chondros, Y., Dimarogonas, A.D. and Yao, J. (1998), "A continuous cracked beam vibration theory", *J. Sound Vib.*, **215**(1), 17-34. https://doi.org/10.1006/jsvi.1998.1640

Fernández-Sáez, J., Morassi, A. and Rubio, L. (2017), "Crack identification in elastically restrained vibrating rods", *Int. J. Non Linear Mech.*, **94**, 257-267. https://doi.org/10.1016/j.ijnonlinmec.2017.03.018

Gairola, S., Rengaswamy, J. and Verma, R. (2023), "A study on XFEM simulation of tensile, fracture toughness, and fatigue crack growth behavior of Al 2024 alloy through fatigue crack growth rate models using genetic algorithm", *Fatigue Fract. Eng. Mater. Struct.*, **46**, 2121-2138. https://doi.org/10.1111/ffe.13987

Kim, H., Yoo, H.H. and Yung, J. (2013), "Dynamic model for free vibration and response analysis of rotating beams", *J. Sound Vib.*, **332**, 5917-5928. https://doi.org/10.1016/j.jsv.2013.06.004

Kindova-Petrova, D. (2022), "A new damage detection index based on beam mode shape slope", *J. Theor. Appl. Mech.*, **52**, 75-87. https://doi.org/10.55787/jtams.22.52.1.075

Krawczuk, M. (1993), "Natural vibration of cracked rotating beams", *Acta Mech.*, **99**, 35-48. https://doi.org/10.1007/BF01177233

Lee, J.W and Lee, J.Y. (2017), "In-plane bending vibration analysis of a rotating beam with multiple edge cracks by using the transfer matrix method", *Meccanica*, **52**, 1143-1157. https://doi.org/10.1007/s11012-016-0449-4

Liu, C. and Yiang, D. (2014), "Crack modeling of rotating blades with cracked hexahedral finite element method", *Mech. Syst. Signal. Process.*, **2**, 406-423. https://doi.org/10.1016/j.ymssp.2014.01.007

Liu, C., Yiang, D. and Chu, F. (2015), "Influence of alternating loads on nonlinear vibration characteristics of cracked blade in rotor system", *J. Sound Vib.*, **353**, 205-219. https://doi.org/10.1016/j.jsv.2015.05.007

Maity, D. and Tripathy, R.R. (2005), "Damage assessment of structures from changes in natural frequencies using genetic algorithm", *Struct. Eng. Mech., Int. J.*, **19**(1), 21-42. https://doi.org/10.12989/sem.2005.19.1.021

Masoud, A.A. and Al-Said, S. (2009), "A new algorithm for crack localization in a rotating Timoshenko beam", *J. Sound Vib.*, **15**(10), 1541-1561. https://doi.org/10.1177/1077546308097272

Matlab (2023), MATLABTM, Optimization toolbox. User's guide.

Mohammed, A.A., Neilson, R.D., Deans, W.F. and MacConnell, P. (2014), "Crack detection in a rotating shaft using artificial neural networks and PSD characterisation", *Meccanica*, **49**, 255-266. https://doi.org/10.1007/s11012-013-9790-z

Muñoz-Abella, B., Rubio, L., Rubio, P. and Montero, L. (2018), "Elliptical crack identification in a nonrotating shaft", *Shock Vib.*, vol. 2018, Article ID 4623035, 10 pages. https://doi.org/10.1155/2018/4623035

Muñoz-Abella, B., Ruiz-Fuentes, A., Rubio, P., Montero, L. and Rubio, L. (2020), "Cracked rotor diagnosis by means of frequency spectrum and artificial neural networks", *Smart Struct. Syst., Int. J.*, **25**(4), 459-469. https://doi.org/10.12989/sss.2020.25.4.459

Muñoz-Abella, B., Rubio, L. and Rubio, P. (2022a), "Closed-form solution for the natural frequencies of low-speed cracked Euler–Bernoulli rotating beams", *Mathematics*, **10**(24), 4742. https://doi.org/10.3390/math10244742

Muñoz-Abella, B., Rubio, L. and Rubio, P. (2022b), "Aplicación de redes neuronales artificiales en la identificación de fisuras en vigas rotatorias Euler-Bernoulli a bajas velocidades", XV Congreso Iberoamericano de Ingeniería Mecánica, Madrid, Spain, November. [In Spanish]

Muñoz-Abella, B., Rubio, L. and Rubio, P. (2023), "Coefficients Cracked rotating beam", Zenodo repository. https://doi.org/10.5281/zenodo.8329047

Nayyar, A., Baneen, U., Naqvi, S.A.Z. and Ahsan, M. (2021), "Detection and localization of multiple small damages in beam", *Adv. Mech. Eng.*, **13**(1). https://doi.org/10.1177/1687814020987329

Özdemir, Ö. and Kaya, M.O. (2006), "Flapwise bending vibration analysis of a rotating tapered cantilever Bernoulli–Euler beam by differential transform method", *J. Sound Vib.*, **1-2**, 413-420. https://doi.org/10.1016/j.jsv.2005.01.055

Ramezani, M. and Bahar, O. (2021), "Structural damage identification for elements and connections using an improved genetic algorithm", *Smart Struct. Syst., Int. J..*, **28**(5), 643-660. https://doi.org/10.12989/sss.2021.28.5.643

Rubio, L. (2009), "An efficient method for crack identification in simply supported Euler–Bernoulli beams", *J. Vib. Acoust.*, **131**(5), 051001 (6 pages). https://doi.org/10.1115/1.3142876

Rubio, L., Fernández-Sáez, J. and Morassi, A. (2018), "A Identification of an open crack in a beam with variable profile by two resonant frequencies", *J. Vib. Control.*, **24**(5), 839-859. https://doi.org/10.1177/1077546316671483

Sekhar, A.S. (2004), "Crack identification in a rotor system: a model-based approach", *J. Sound Vib.*, **270**(4-5), 887-902. https://doi.org/10.1016/S0022-460X(03)00637-0

Suh, M.W., Yu, J.M. and Lee, J.H. (2000), "Crack identification using classical optimization technique", *Key Eng. Mater.*, **183-187**, 61-66. https://doi.org/10.4028/www.scientific.net/KEM.183-187.61

Talebi, S. and Ariaei, A. (2015), "Vibration analysis of a rotating Timoshenko beam with internal and external flexible connections", *Arch. Appl. Mech.*, **85**, 555-572. https://doi.org/10.1007/s00419-014-0930-2

Valverde-Marcos, B., Muñoz-Abella, B., Rubio, P. and Rubio, L. (2022), "Influence of the rotation speed on the dynamic behaviour of a cracked rotating beam", *Theor. Appl. Fract. Mech.*, **117**, 103209. https://doi.org/10.1016/j.tafmec.2021.103209

Wauer, J. (1991), "Dynamics of cracked rotating blades", *Appl. Mech. Rev.*, **44**(11S), S273-S278. https://doi.org/10.1115/1.3121364

Yang, L.H., Yang, Z.S., Mao, Z., Wu, S.M., Chen, X.F. and Yan, R.Q., (2021a), "Dynamic characteristic analysis of rotating blade with transverse crack—Part I: modeling, modification, and validation", *J. Vib. Acoust.*, **143**(5), 051010 (15 pages). https://doi.org/10.1115/1.4049385

Yang, L.H., Yang, Z.S., Mao, Z., Wu, S.M., Chen, X.F. and Yan, R.Q., (2021b), "Dynamic characteristic analysis of rotating blade with transverse crack—Part II: A comparison study of different crack models", *J. Vib. Acoust.*, **143**(5), 051011 (13 pages). https://doi.org/10.1115/1.4049386

Yashar, A., Ferguson, N. and Ghandchi-Tehrani, M. (2018), "Simplified modelling and analysis of a rotating Euler-Bernoulli beam with a single cracked edge", *J. Sound Vib.*, **420**, 346-356. https://doi.org/10.1016/j.jsv.2017.12.041

Yazdanpanah, O., Seyedpoor, S.M. and Akbarzadeh-Bengar, H. (2015), "A new damage detection indicator for beams based on mode shape data", *Struct. Eng. Mech., Int. J.*, **53**(4), 725-744. https://doi.org/10.12989/sem.2015.53.4.725